

UNIVERSITY OF SOUTHAMPTON
INSTITUTE OF SOUND AND VIBRATION RESEARCH
SIGNAL PROCESSING & CONTROL GROUP

A Linear Model for Random Tyre Excitation and its Active Control

by

S J Elliott and E Rustighi

ISVR Technical Memorandum N° 945

February 2005

Authorised for issue by
Prof S J Elliott
Group Chairman

ACKNOWLEDGEMENT

The work of E.Rustighi is supported by the EU under the integrated project "Integrated materials for active noise reduction", InMAR. We would also like to thank S.Finnveden of KTH for stimulating conversations in this area.

CONTENTS

	<u>Page</u>
Abstract	v
1. Introduction	1
2. Description of the contact forces	2
3. Response of the tyre	4
4. Soundfield inside the vehicle	9
5. Active control	11
6. Simulation example	15
6.1 Model of the tyre	15
6.2 The Winkler elastic foundation	17
6.3 Expression of the road roughness	18
6.4 The kinetic energy	20
6.5 The application of the optimal control filter	21
7. Conclusions	23
A. A brief explanation of some ring models	24
References	28

FIGURES

	<u>Page</u>
Figure 1. The radial velocities of the force tyre, v_T , suspended off the road, are related to the applied forces, f_T , via the mobility matrix Y_F (left hand figure). When the tyre is resting on the road (right hand figure), a Winkler bedding model of the contact patch is used, excited by the displacements of the road, d , and generating vertical displacements of the tyre in the contact patch, w	29
Figure 2. Block diagram for the active control formulation.	29
Figure 3. Effect of the road contact on the tyre point mobility calculated in the middle of the contact patch (a) and opposite to the contact patch (b): — hanged tyre; - - - tyre on ground.	30
Figure 4. Expected value of the kinetic energy, shown in the form of power spectrum density (a) and one-third octave bands (b), evaluated at different car speeds: · · · 50 km/h; — 35 km/h; - - - 20 km/h.	31
Figure 5. Expected value of the kinetic energy, shown in the form of power spectrum density (a) and one-third octave bands (b) for a speed of 35 km/h: — controller off, · · · uniform control on and - - - multi dof control on.	32
Figure 6. Modelling of the different kinds of actuators: distributed force actuator (a), strain actuator (b) and acoustic actuator (c).	33
Figure 7. Influence of the position of the actuator on reduction of the global kinetic energy.....	33

TABLES

	<u>Page</u>
Table 1. Material parameters for the ring model of the tyre.	16
Table 2. Constant c for road profile spectral density expressed in $m^3/cycles$ when n is in cycles/m (Robson, 1979).	19

ABSTRACT

A linear model is presented for the elemental response of a tyre excited by forces in the contact patch. Although the mechanism of the contact dynamics is, in general, nonlinear, it is assumed here that the tyre is soft enough for the whole of the contact patch to remain in touch with the road, in which case a linear model can be used to calculate the contact forces from the road roughness and the resulting radial velocity of the tyre. The velocities are described by their spectral density matrix, which is then used to calculate the expectation of the tyre's kinetic energy and sound power radiation. The sum of squared pressures inside the vehicle can be calculated in a similar way. A formulation is also presented for calculating the optimal performance when controllable secondary force distributions also act on the tyre to implement active control. Simple two-dimensional simulations are presented to illustrate the practical use of the formulation.

1. Introduction

A simple linear model is presented for the random excitation of a tyre's vibration and its subsequent sound radiation. The excitation of the tyre as it runs over a rough road is modelled as a random displacement distribution with a specified spatial correlation. This is used to calculate the forces at a grid of discrete points in the contact patch. The spectral density matrix for the vector of radial velocities at each point on this grid is then calculated from the structural mobility matrix for the dynamics of the tyre supported on the contact patch.

The spectral density matrix for the road roughness and the tyre's mobility matrix could, in principle, be determined experimentally. It is more likely that theoretical models will be used to estimate these quantities, however. A complete contact model would need to be nonlinear to account for the fact that only part of the tyre in the contact patch connects with the road surface. The simplified linear model used here can be obtained by assuming that the tyre is smooth and soft enough that the whole of the tyre's surface in the contact patch connects with the road. In this case the spectral density matrix for the contact forces can be calculated from a statistical model of the road roughness using a linear analysis.

The kinetic energy associated with the radial motion of the tyre and the sound power radiated by the tyre are then calculated. The structure-borne sound inside the vehicle is also calculated from the tyre's mechanical impedance matrix, from tyre velocities to hub forces, and the vehicle's acoustic impedance matrix, from hub forces to internal pressures.

The effect of a controllable, secondary, force distribution is then considered. In order to determine the physical limits of control with various secondary actuators, a feedforward control strategy is assumed, with perfect knowledge of the forces in the contact patch. A formulation is presented for calculating the control forces required to minimise a quadratic cost function such as the radiated or internal sound field. These can then be substituted back into the model to estimate the physical effects of different active control strategies. Preliminary simulation results are presented for a 2D model to illustrate the use of the formulation presented.

2. Description of the Road Excitation

The vibration of a tyre generated by its rolling over a rough road is an important source of internal and external vehicle noise at low frequencies. The interaction between the tyre tread and the rough road generates a time-varying force distribution over the contact patch. If the contact patch is divided into a fine grid, the force distribution can be approximated by a vector of forces acting at the elements defined by the grid. Each force will have a random time history, which we will assume to be stationary, with its own autocorrelation function and a set of cross-correlation functions with the other forces acting in the contact patch. This spatial correlation partly arises because the road surface roughness will have a distribution of lengthscales and the larger peaks will be in contact with the tyre over a significant distance.

The road roughness itself is a random variable whose properties vary with the type of road surface, as described by Dodds and Robson (1973) and Robson (1979) for example. The statistical properties of the road surface displacement can be described by its spatial correlation function or its wavenumber spectrum, which Dodds and Robson suggest falls off in approximate inverse proportional to the square of the wavenumber. These authors also discuss experimental evidence for the roughness being approximately homogeneous and isotropic and they develop a two-dimension Gaussian model.

In this report we assume that the road roughness is described by a vector of displacements at each of a set of N_C points on a grid in the contact patch. A frequency-domain formulation will be used so that each displacement variable, d_1 to d_{N_C} , corresponds to the Fourier transform of a long time history, although the explicit dependence on frequency, ω , will be suppressed for notational convenience. The individual complex displacements are grouped together in an $N_C \times 1$ vector, \mathbf{d} , equal to $[d_1, d_2 \cdots d_{N_C}]^T$ and the spectral density matrix of the road displacement is then defined to be

$$\mathbf{S}_{dd} = E[\mathbf{d}\mathbf{d}^H], \quad (2.1)$$

where E denotes the expectation operator and the subscript ^H denotes the Hermitian, complex conjugate, transpose. The diagonal elements of \mathbf{S}_{dd} correspond to the power spectral densities of each of the displacements, which will be assumed to be equal in this model, and the off-diagonal terms correspond to cross spectral densities between the displacement at different points. A similar formulation has been used to specify the random pressure distributions caused by a turbulent boundary layer, see for example Elliott et al. (2004). It is interesting to note that the influence of one piece of road surface as it passes from one end of the contact patch to another will generate a similar delay in the cross spectral densities as the convection in a turbulent boundary layer.

It would be very convenient if a stochastic description could also be developed for the tyre contact forces, using a contact model. In general, however, the contact model is rather complicated because not all of the tyre does come into contact with the road. Iterative approaches to solving this nonlinear problem are discussed, for example, by Larsson (2002) and Kropp et al. (2004). One simplifying assumption that could be made is that the contact stiffness is generated only by a set of isolated, locally-acting, springs, which is called a Winkler bedding (Johnson, 1985). The compression of the springs will depend on the curvature of the tyre, the road roughness and the vibration of the tyre belt. The vibration will depend on the forces acting over the whole contact patch and this, in turn, will influence which parts of the tyre are in contact with the road and which are not. An iterative solution to this contact problem is discussed by Larsson (2002), whereby the contact points are initially calculated at one instant in time assuming that the contact forces are zero. A force distribution is then calculated from the tyre dynamics for the points assumed to be in contact. Some places will be calculated as having a negative contact force, however, which clearly are not in contact. At the next iteration these points are removed from the set of contact points and the forces recalculated.

In this way a time-history of the contact force at each point in the contact patch can be calculated for a tyre with a specific tread pattern rolling over a specific piece of rough road, Kropp et al. (2004). Different time histories would be generated if the tyre tread was slightly rotated with respect to the road before the calculation began.

The statistical properties of this force distribution do not seem to have been calculated. Long simulations would be necessary to obtain time histories of sufficient length to calculate accurate correlation functions from the force time histories. It would, however, be very interesting to compare these calculated correlation functions with the scaled versions of the spatial correlation function of the road surface itself and to investigate how they changed with load, tread and tyre pressure.

In this report a very simplified contact model will be used in which it is assumed that all of the contact patch is in touch with the road at all times. Such an approximation would hold in the limiting case of a smooth soft tyre travelling over a road which is not too rough, such that the road displacement is small compared with the static compression of the tyre in the contact patch. This contact model has the important advantage that the interaction between the road roughness and the tyre vibration is then linear. In the following section a matrix formulation is presented to calculate the spectral density matrix of the tyre's vibration when driven by a road roughness specified by the spectral density matrix of road displacements in equation (2.1), and its consequent kinetic energy and sound power radiation.

3. Response of the Tyre

The tyre tread and sidewall are assumed to be divided up into N_T discrete elements, as shown in Figure 1. This array of elements includes those in the contact patch, described in Section 2, as a subset. The vector of complex radial velocities at the centre of each element, \mathbf{v}_T , are assumed to be related to the vector of all the complex forces acting on the elements, \mathbf{f}_T , via a matrix of structural mobilities for the free tyre suspended off the ground, \mathbf{Y}_F , so that

$$\mathbf{v}_T = \mathbf{Y}_F \mathbf{f}_T. \quad (3.1)$$

Figure 1(a) shows the array of forces and velocities for a 2D model of the tyre. Although the hub is initially assumed to be fixed when calculating the "free" response of the tyre in equation (3.1), an analysis exactly analogous to that outlined below could be used to incorporate the finite mechanical impedance of the vehicle

suspension into the tyre dynamics. The number and distribution of the elements will depend on the frequency range of interest, and their density will typically be chosen to be six times the smallest wavelength of interest. Such a model is primarily of use at lower frequencies, below about 400Hz, at which the external sound radiation from the tyre and the internal sound generation are dominated by the tyre's vibration rather than aerodynamic sources, Kropp (2004). The distribution of elements in the contact patch of the tyre could be more dense than over the rest of the tread and sidewall, since the spatial wavelengths of the excitation due to the tyre running over a rough road could be smaller than those of any other excitation.

The tyre is then assumed to be in contact with the road using the linear contact model described above, which gives rise to the vector of driving forces, \mathbf{f}_T . In principle the distribution of forces could represent both the distribution of primary driving forces due to road interaction in the contact patch and the distribution of secondary forces introduced in an attempt to control the vibration of the tyre. A discussion of such active control techniques will be postponed until a later section, however, and we will initially concentrate on excitation only due to the forces caused by the interaction between the road and the tyre in the contact patch. In the simplest case, shown in Figure 1(b), such a model consists of a Winkler bedding of N_C independent springs that connect each point on the road with vertical displacement of d_1 to d_{N_C} to each point in the contact patch on the tyre, with vertical tyre displacement w_1 to w_{N_C} , which are assumed to be equal to the radial tyre displacements since the contact patch is only small.

The force at all N_T points on the tyre is related to the difference between the road and tyre displacements by the linear equation

$$\mathbf{f}_T = \mathbf{K}_{TC}(\mathbf{d} - \mathbf{w}), \quad (3.2)$$

where \mathbf{d} and \mathbf{w} are $N_C \times 1$ vectors of the vertical displacement of the road and tyre in the contact patch and \mathbf{K}_{TC} is an $N_T \times N_C$ matrix describing the linear contact stiffness. In the case of a Winkler bedding, \mathbf{K}_{TC} has N_C elements equal to the individual contact stiffnesses on the diagonal, and the other elements are zero.

The displacement of the tyre in the contact patch caused by these forces is now written as

$$\mathbf{w} = \mathbf{C}_{CT} \mathbf{f}_T \quad (3.3)$$

where \mathbf{C}_{CT} is the $N_C \times N_T$ matrix of tyre compliances at the points in the contact patch. These compliances can be calculated as a subset of the mobilities in equation (3.1), divided by $j\omega$.

Substituting equation (3.3) into equation (3.2), and assuming that the matrix $[\mathbf{I} + \mathbf{K}_{TC} \mathbf{C}_{CT}]$ is not singular, allows the forces on the tyre due to the road displacements \mathbf{d} to be expressed as

$$\mathbf{f}_T = [\mathbf{I} + \mathbf{K}_{TC} \mathbf{C}_{CT}]^{-1} \mathbf{K}_{TC} \mathbf{d}. \quad (3.4)$$

The vector of radial velocities for the tyre due to the road roughness can then be calculated from equation (3.1) as

$$\mathbf{v}_T = \mathbf{Y}_F [\mathbf{I} + \mathbf{K}_{TC} \mathbf{C}_{CT}]^{-1} \mathbf{K}_{TC} \mathbf{d} \quad (3.5)$$

which may be written in more compact form as

$$\mathbf{v}_T = \mathbf{T} \mathbf{d} \quad (3.6)$$

where the overall transfer matrix, \mathbf{T} , is equal to $\mathbf{Y}_F [\mathbf{I} + \mathbf{K}_{TC} \mathbf{C}_{CT}]^{-1} \mathbf{K}_{TC}$.

The spectral density matrix of the tyre's velocities can be defined in an analogous manner to equation (2.1) as

$$\mathbf{S}_{vv} = E \left[\mathbf{v}_T \mathbf{v}_T^H \right]. \quad (3.7)$$

Using equation (3.6), this can be expressed in terms of the spectral density matrix of road displacements, \mathbf{S}_{dd} in equation (2.1), as

$$\mathbf{S}_{vv} = \mathbf{T} \mathbf{S}_{dd} \mathbf{T}^H. \quad (3.8)$$

The kinetic energy associated with the radial motion of the tyre is proportional to the inner product of the vector of velocities weighted by the mass matrix \mathbf{M} . The expectation of the tyre's radial kinetic energy can thus be expressed as

$$E_{\text{kinetic}} = E[\mathbf{v}_T^H \mathbf{M} \mathbf{v}_T] \quad (3.9)$$

and since E_{kinetic} is a scalar, the trace of equation (3.9) can be taken, which can be rearranged to give

$$E_{\text{kinetic}} = \text{trace}[\mathbf{M} \mathbf{S}_{vv}]. \quad (3.10)$$

Once the radial velocities at each element have been specified, the complex sound pressure at any point on the surface of the tyre can be also calculated using a set of acoustic radiation impedances. It is assumed that these acoustic pressures at the surface of the tyre generate a far lower response than the force vector, \mathbf{f}_T , and so the sound radiation can be calculated from a weakly coupled analysis. The sound radiated by a structure divided into elements each vibrating with a velocity given by an element of \mathbf{v}_T , is then given by

$$W_{\text{sound}} = \mathbf{v}_T^H \mathbf{R}_A \mathbf{v}_T, \quad (3.11)$$

where \mathbf{R}_A is half the acoustic radiation resistance matrix. This matrix can, in principle, be measured as discussed by Koopman and Farelane (1997) or calculated for a given geometry of structure, radiating into a particular environment. In the case of interest here, it could be assumed that the vibration of the tyre in the contact patch makes no contribution to the radiated sound power. The relevant parts of the

radiation resistance matrix would then be set to zero, without altering the form of equation (3.11).

Taking the expectation of equation (3.11) and again using the properties of the trace function, the radiated sound power can be expressed in terms of the velocity spectral density matrix as

$$W_{\text{sound}} = \text{trace} [\mathbf{R}_A \mathbf{S}_{vv}] . \quad (3.12)$$

It would be interesting to compare the radiated sound power with the power supplied to the tyre by the motion over the road. This may be calculated from half the real part of the sum of products of the complex forces on the tyre and the subsequent complex velocities, and may be denoted W_{supplied} , so that

$$W_{\text{supplied}} = \frac{1}{2} \text{Re} [\mathbf{v}_T^H \mathbf{f}_T] . \quad (3.13)$$

If the matrix of tyre mobilities given in equation (3.1) is invertible, the vector of forces, \mathbf{f}_T , may be written as $\mathbf{Y}_F^{-1} \mathbf{v}_T$. This allows the power supplied to the tyre to be written as

$$W_{\text{supplied}} = \frac{1}{2} \text{Re} [\mathbf{v}_T^H \mathbf{Y}_F^{-1} \mathbf{v}_T] = \mathbf{v}_T^H \mathbf{R}_F \mathbf{v}_T . \quad (3.14)$$

where $\frac{1}{2} \text{Re} [\mathbf{Y}_F^{-1}]$ is defined to be \mathbf{R}_F , which has been assumed to be symmetrical due to reciprocity, although this assumption may have to be revisited for a rotating tyre.

Taking expectations of equation (3.14) and again using the properties of the trace function, the power supplied to the tyre by the motion on the road can finally be written in terms of its velocity spectral density matrix as

$$W_{\text{supplied}} = \text{trace} [\mathbf{R}_F \mathbf{S}_{vv}] \quad (3.15)$$

4. Sound Field Inside the Vehicle

The internal sound field in the vehicle is assumed to be entirely structure-borne in this low-frequency model, and to be excited by the vibration of the tyre hub. If the tyre hub behaves as a rigid body then there are six force components that need to be specified, corresponding to three linear forces and three moments. These complex forces can be represented as the elements of the vector \mathbf{f}_H , and are assumed to be generated by the vibration of the tyre, with radial velocities \mathbf{v}_T . Note that \mathbf{v}_T has been calculated from the tyres "free" mobility matrix, \mathbf{Y}_F in equation (3.1), which could incorporate the effects of a compliant connection from the vehicles suspension system at the wheel hub, but for simplicity this connection is assumed here to be rigid. The linear transformation from the radial velocities to the hub forces, which is governed by the tyre's dynamics, is represented by a mechanical impedance matrix \mathbf{Z}_{HT} , so that

$$\mathbf{f}_H = \mathbf{Z}_{HT} \mathbf{v}_T . \quad (4.1)$$

The acoustic pressures at a set of points inside the vehicle are represented as the complex elements of the vector \mathbf{p}_I . These are assumed to be generated by the hub forces, \mathbf{f}_H , by a matrix of complex impedances, \mathbf{Z}_{IH} , that represent both the structural response of the vehicle and the acoustic response of its interior. The internal pressures are thus given by

$$\mathbf{p}_I = \mathbf{Z}_{IH} \mathbf{f}_H . \quad (4.2)$$

The response of the tyre in equation (4.1) can be combined with the response of the vehicle in equation (4.2) to give the internal pressures as a function of the tyre's velocities

$$\mathbf{p}_I = \mathbf{Z}_{IT} \mathbf{v}_T \quad (4.3)$$

where \mathbf{Z}_{IT} is equal to $\mathbf{Z}_{IH} \mathbf{Z}_{HT}$.

A useful representation of the average acoustic pressure inside the vehicles is the sum of the squared pressures at a set of points. These points can be concentrated near the ears of the driver, or they can be more uniformly distributed throughout the vehicle cabin. In the latter case, then as the number of microphones becomes large compared with the number of acoustic modes in the cabin, the sum of squared pressures becomes proportional to the total acoustic potential energy.

If we define the spectral density matrix for the pressures as

$$\mathbf{S}_{pp} = E[\mathbf{p}_1 \mathbf{p}_1^H] , \quad (4.4)$$

then the sum of squared pressures is given by

$$P_{\text{internal}} = \text{trace}[\mathbf{S}_{pp}] . \quad (4.5)$$

Using equation (4.3) and the properties of the trace operation, the sum of square pressures can be represented as a function of the spectral density matrix of the tyre's velocities, \mathbf{S}_{vv} , as

$$P_{\text{internal}} = \text{trace}[\mathbf{Z}_{IT}^H \mathbf{Z}_{IT} \mathbf{S}_{vv}] . \quad (4.6)$$

5. Active Control

We now consider the case in which an additional set of controllable forces act on the tyre to implement active control. Two key assumptions in this analysis are that the system is linear and that we have chosen a set of variables for which we can apply superposition. We have seen in Section 3 that if there are no controllable forces on the tyre, its velocity depends on the road roughness according to equation (3.6). We now consider the case in which there is no road roughness but the velocity is due to the controllable, secondary, forces. The effect on the velocity of both road roughness and secondary forces can then be calculated by superposition.

The total force on the tyre resting on the road surface in Figure 1(b) due to a vector of N_S secondary forces, \mathbf{f}_S , with $\mathbf{d} = 0$, will be due to the effect of \mathbf{f}_S directly and also due to contact forces that arise because of the resulting motion of the tyre. The vector of forces can thus be written as

$$\mathbf{f}_T = \mathbf{T}_S \mathbf{f}_S - \mathbf{K}_{TC} \mathbf{w}, \quad (5.1)$$

where \mathbf{T}_S is an $N_T \times N_S$ matrix that defines how each secondary force acts on the grid of elements we have chosen for the tyre. Typically a secondary force may act across several of these elements. Although a mechanical secondary excitation is assumed here, a similar formulation could also be used to include acoustic secondary forces inside the tyre.

The second term in equation (5.1) is due to the fact that the secondary force will cause the tyre to vibrate and generate a displacement \mathbf{w} in the contact patch. As in Section 3, this displacement depends on the compliance of the tyre and may be written as

$$\mathbf{w} = \mathbf{C}_{CT} \mathbf{f}_T. \quad (5.2)$$

Substituting equation (5.2) into (5.1) and solving for \mathbf{f}_T , assuming again that the matrix $[\mathbf{I} + \mathbf{K}_{TC} \mathbf{C}_{CT}]$ is not singular, we obtain

$$\mathbf{f}_T = [\mathbf{I} + \mathbf{K}_{TC} \mathbf{C}_{CT}]^{-1} \mathbf{T}_S \mathbf{f}_S. \quad (5.3)$$

The vector of tyre velocities due to the secondary excitation can thus be expressed, using equation (3.1), as

$$\mathbf{v}_T = \mathbf{Y}_F [\mathbf{I} + \mathbf{K}_{TC} \mathbf{C}_{CT}]^{-1} \mathbf{T}_S \mathbf{f}_S. \quad (5.4)$$

If we now denote the vector of tyre velocities due to the road roughness only as \mathbf{v}_p , which from equation (3.6) is equal to $\mathbf{T}\mathbf{d}$, and define the overall mobility from the secondary excitation to the velocity vector, which from equation (5.4) is equal to

$\mathbf{Y}_F[\mathbf{I} + \mathbf{K}_{TC} \mathbf{C}_{CT}]^{-1} \mathbf{T}_s$, as \mathbf{Y} , then the nett velocity due to both the road roughness and secondary excitation must be

$$\mathbf{v}_T = \mathbf{v}_P + \mathbf{Y} \mathbf{f}_S. \quad (5.5)$$

In this initial investigation a feedforward control strategy will be assumed and, for simplicity, the analysis is performed in the frequency domain without the constraint of causality (Elliott, 2001). The secondary forces are assumed to be driven from a set of N_R reference signals, contained in the vector \mathbf{x} , which is correlated in some way to the road displacements, \mathbf{d} . These reference signals are passed through a matrix of $N_S \times N_R$ filters with frequency response \mathbf{W} so that

$$\mathbf{f}_S = \mathbf{W} \mathbf{x}. \quad (5.6)$$

Combining the definition of \mathbf{v}_P in equation (3.6) with equations (5.5) and (5.6), the vector of tyre velocities can be written as

$$\mathbf{v}_T = \mathbf{T} \mathbf{d}_P + \mathbf{Y} \mathbf{W} \mathbf{x}. \quad (5.7)$$

The block diagram for this arrangement is shown in Figure 2. The matrix of control filters, \mathbf{W} , will now be calculated which minimises a quadratic cost function of the form

$$J = \text{trace}(\mathbf{Q} \mathbf{S}_{vv}). \quad (5.8)$$

Note that the tyre's radial kinetic energy, equation (3.10), the sound power it radiates, equation (3.12), or the internal pressure in the vehicle, equation (4.6), can all be expressed in the form of equation (5.8) with a suitable choice of the Hermitian weighting matrix \mathbf{Q} .

Since \mathbf{S}_{vv} is defined to be $E[\mathbf{v}_T \mathbf{v}_T^H]$ in equation (3.7), and using the properties of the trace operator, the cost function in equation (5.8) can be written as

$$J = \text{trace } E[\mathbf{v}_T^H \mathbf{Q} \mathbf{v}_T]. \quad (5.9)$$

If the vector of velocities has the form given by equation (5.7), then the cost function becomes

$$J = E\left[\left(\mathbf{x}^H \mathbf{W}^H \mathbf{Y}^H + \mathbf{T}^H \mathbf{d}^H\right) \mathbf{Q} (\mathbf{T} \mathbf{d} + \mathbf{Y} \mathbf{W} \mathbf{x})\right] \quad (5.10)$$

which can in turn be written as

$$J = \text{trace} \left[\mathbf{W}^H \mathbf{Y}^H \mathbf{Q} \mathbf{Y} \mathbf{W} \mathbf{S}_{xx} + \mathbf{W}^H \mathbf{Y}^H \mathbf{Q} \mathbf{T} \mathbf{S}_{xd} + \mathbf{S}_{xd}^H \mathbf{T}^H \mathbf{Q} \mathbf{Y} \mathbf{W} + \mathbf{T}^H \mathbf{Q} \mathbf{T} \mathbf{S}_{dd} \right] \quad (5.11)$$

where $\mathbf{S}_{xx} = E[\mathbf{x} \mathbf{x}^H]$, $\mathbf{S}_{xd} = E[\mathbf{d} \mathbf{x}^H]$ and $\mathbf{S}_{dd} = E[\mathbf{d} \mathbf{d}^H]$.

Differentiating equation (5.11) with respect to the real and imaginary parts of \mathbf{W} , which are denoted \mathbf{W}_R and \mathbf{W}_I , gives the matrix of complex gradients (Elliott, 2001)

$$\frac{\partial J}{\partial \mathbf{W}_R} + j \frac{\partial J}{\partial \mathbf{W}_I} = 2 \left[\mathbf{Y}^H \mathbf{Q} \mathbf{Y} \mathbf{W} \mathbf{S}_{xx} + \mathbf{Y}^H \mathbf{Q} \mathbf{T} \mathbf{S}_{xd} \right]. \quad (5.12)$$

Finally the optimum least-square control filter matrix can be obtained by setting equation (5.12) to zero, and provided that the matrices $\mathbf{Y}^H \mathbf{Q} \mathbf{Y}$ and \mathbf{S}_{xx} are not singular, we obtain

$$\mathbf{W}_{\text{opt}} = - \left[\mathbf{Y}^H \mathbf{Q} \mathbf{Y} \right]^{-1} \mathbf{Y}^H \mathbf{Q} \mathbf{T} \mathbf{S}_{xd} \mathbf{S}_{xx}^{-1}. \quad (5.13)$$

In practice, there may be considerably fewer reference signals than uncorrelated components in the primary force. In order to calculate the performance under ideal conditions, however, we can assume that a sufficiently large number of reference signals is used, so that the primary road disturbances can be exactly generated from the reference signals, via the filter \mathbf{P} , so that

$$\mathbf{S}_{xd} \mathbf{S}_{xx}^{-1} = \mathbf{P}. \quad (5.14)$$

To further simplify the problem we can assume that the primary road displacements themselves, \mathbf{d} , could be used as reference signals, in which case $\mathbf{S}_{xd} \mathbf{S}_{xx}^{-1}$ would equal an identity matrix, so that

$$\mathbf{W}_{\text{opt}} = -[\mathbf{Y}^H \mathbf{Q} \mathbf{Y}]^{-1} \mathbf{Y}^H \mathbf{Q} \mathbf{T}. \quad (5.15)$$

Using equations (5.6) and (5.15), the secondary force is then

$$\mathbf{f}_s = -[\mathbf{Y}^H \mathbf{Q} \mathbf{Y}]^{-1} \mathbf{Y}^H \mathbf{Q} \mathbf{T} \mathbf{d}. \quad (5.16)$$

The total velocity of the loaded tyre can thus be calculated from equation (5.5), and using the fact that $\mathbf{T} \mathbf{d}$ is equal to \mathbf{v}_p , as

$$\mathbf{v}_T = \left[\mathbf{I} - \mathbf{Y} [\mathbf{Y}^H \mathbf{Q} \mathbf{Y}]^{-1} \mathbf{Y}^H \mathbf{Q} \right] \mathbf{v}_p, \quad (5.17)$$

The tyre's kinetic energy or radiated sound power after active control can be calculated using the results from Section 3, and the interior mean square pressure after control can be calculated using the results of Section 4.

6. Simulation Example

6.1 Model of the Tyre

In this section a simple two-dimensional model of the tyre is used to generate some illustrative results from the theory outlined below. Such a model can be used to account for the ring modes of the tyre that dominate its response below about 400 Hz.

The tyre was been modelled as a stationary ring resting on a massless foundation characterised by two spring constants, k_r and k_θ . A constant pressure, P_0 acts around the ring in order to take into account the inflation pressure of the tyre. The dynamics of a stationary ring are expressed by the following two equations (Huang and Soedel, 1987, Soedel, 1993):

$$\frac{D}{a^4}(u_r''' - u_\theta''') - \frac{K}{a^2}(u_r' + u_\theta'') + \frac{P_0}{a}(u_\theta - 2u_r' - u_\theta'') + k_\theta u_\theta + \rho h \ddot{u}_\theta = q_\theta, \quad (6.1)$$

$$\frac{D}{a^4}(u_r''' - u_\theta''') + \frac{K}{a^2}(u_r + u_\theta') + \frac{P_0}{a}(u_r + 2u_\theta' - u_r'') + k_r u_r + \rho h \ddot{u}_r = q_r - P_0, \quad (6.2)$$

where a is the radius of the wheel, h is its thickness, $D = Eh^3/12$ is the bending stiffness, $K = Eh$ is the membrane stiffness, ρ is the density, E is the Young's modulus, P_0 is the internal pressure, k_r and k_θ are the radial and tangential bedding stiffnesses, q_r and q_θ are the distributed radial and tangential forces and, u_r and u_θ are the radial and the tangential displacements. Derivatives with respect to the angle θ are indicated by primes whereas derivatives with respect to the time are indicated by dots.

Material losses have been introduced by the imaginary parts of the stiffness parameters k_r , k_θ , K and D and the imaginary part of the internal pressure P_0 , where the loss factors have been indicated respectively by η_r , η_θ , η_m , η_b and η_p . Appendix A provides further explanation of the model.

Table 1. Material parameters for the ring model of the tyre.

Description and dimensions	Constant	Value
Radius of the tyre [m]	a	0.33
Tyre thickness [m]	h	0.02
Tyre width [m]	b	0.11
Young's modulus [Pa]	E	4.90×10^8

Tyre density [kg/m ³]	ρ	1000
Tangential bedding coefficient [N/m ³]	k_t	8.82×10^6
Radial bedding coefficient [N/m ³]	k_r	1.09×10^6
Rubber Poisson ratio	ν	0.45
Internal Pressure [Pa]	P_0	2.00×10^5
Loss Factor radial stiffness	η_r	0.05
Loss Factor tangential stiffness	η_t	0.05
Loss Factor longitudinal waves	η_m	0.2
Loss Factor bending waves	η_k	0.3
Loss Factor pressure tension	η_p	0.05
Contact Rubber stiffness [Pa]	k_r	1.00×10^5
Radial segments	N_r	92
Number of modes	N_m	15
Number of contact points	N_c	31
Velocity [Km/h]	V	35

Substituting a trial solution for the motion into equation for the ring dynamics, it is possible to obtain the natural frequencies and the mode shapes of the system (see appendix A for details). The mode shapes can be mass normalised and gathered in the mode shape matrix Ψ . Values for the parameters of the tyre dynamics equations have been inferred from Heckl (1986) and Kropp (1989) and are shown in table 1.

6.2. *The Winkler Elastic Foundation*

The contact between two compliant bodies can be simplified by the use of the Winkler elastic foundation. The tyre and the road can be considered as rigid bodies and the tyre is assumed to be covered by an elastic layer of thickness h and elastic modulus K . There is no interaction between the springs of the foundation, i.e. shear between adjacent elements is ignored. Considering the equations related to two long

cylinders the relationship between the load P and the contact half-width a can be derived to be (Johnson, 1985)

$$a = \sqrt[3]{\left(\frac{3}{2} \frac{hR}{Kb}\right)P}, \quad (6.3)$$

where R is the relative radius of curvature of the two bodies and b the depth of the bodies (tyre width).

Given the width of the contact, the bedding model must be discretised in order to obtain a group of spring connected in parallel. The stiffness of each spring is given by

$$k_s = \frac{K \Delta x_s b}{h}, \quad (6.4)$$

where Δx_s is the width of each spring or the distance between two springs.

The model used here had 31 elements in the contact patch ($N_c = 31$), although doubling this number had negligible effect on the response below 400 Hz. Sixty one additional points were used to specify the response in the remainder of the tread, so that the total number of points used to specify the tyre's response, N_T , was 92 in this case.

The tyre model described by equation (6.1) has been solved to give the forced vibration response of the suspended tyre with a fixed hub, and hence the matrix of mobilities defined by equation (3.1). Using the Winkler bedding model, the forced response of the tyre when placed on the road has also been calculated using equation (5.4). Figure 3 shows the dynamic behaviour of the suspended tyre and the tyre in contact with the road. The contact dynamics mainly affect the response of the first two modes, which are due to the rigid body mass of the tyre on the sidewall stiffness and the first flexible tyre mode respectively.

6.3. Expression of the Road Roughness

For a vehicle travelling at a constant velocity, the imposed displacement may be considered as a realization of a multi-variate stationary random process and so may be described by a spectral density matrix, as discussed in Section 3. Each contact point travels over the same profile as that of the forward contact points, so that each point experiences, after a speed-dependent delay, the same imposed displacement.

The time varying road displacement $d(t)$ is derived from traversing, at velocity v , a rigid road profile which has the form $\hat{d}(x)$, where x indicates position in the direction of motion. At any instant these two quantities must be equal and so the corresponding spectral densities matrices can be expressed as (Robson, 1979, Newland, 1984)

$$S_d(f) = \frac{1}{v} S_{\hat{d}}(n), \quad (6.5)$$

where n is the wave number. It is clear that the spectral density matrix for the wave number transform of $\hat{d}(x)$, $S_{\hat{d}}(n)$, provides an invariant description of a road profile, from which the excitation spectral density matrix $S_d(f)$ can always be derived for any particular vehicle velocity. The road spectral matrix can be described by the following single slope spectrum of the form (Robson, 1979)

$$S_{\hat{d}}(n) = c |n|^{-2.5}, \quad (6.6)$$

with the value of c given in the table 2. In the simulation the mean value given for principal roads has been used.

The point spectral density in the frequency domain can then be expressed as

$$S_d(f) = \frac{c}{v} \left(\frac{f}{v} \right)^{-2.5}. \quad (6.7)$$

The cross spectral density between two points, placed at a distance Δx , may be expressed by

$$S_{12} = S_d e^{-j\omega \frac{\Delta x}{v}}, \quad (6.8)$$

where the road profile is moving from the first point towards the second one. It follows that the spectral density matrix of the displacements at the contact points is given by

$$\mathbf{S}_{dd} = \begin{bmatrix} S_d & S_d e^{j\omega \frac{\Delta x_1}{v}} & S_d e^{j\omega \frac{(\Delta x_1 + \Delta x_2)}{v}} & & \\ S_d e^{-j\omega \frac{\Delta x_1}{v}} & S_d & S_d e^{j\omega \frac{\Delta x_2}{v}} & \dots & \\ S_d e^{-j\omega \frac{(\Delta x_1 + \Delta x_2)}{v}} & S_d e^{-j\omega \frac{\Delta x_2}{v}} & S_d & & \\ & \vdots & & \ddots & \end{bmatrix}. \quad (6.9)$$

Table 2. Constant c for road profile spectral density expressed in m^3/cycles when n is in cycles/m (Robson, 1979).

	Range	Mean
Motorway	$3 \times 10^{-8} - 50 \times 10^{-8}$	10×10^{-8}
Principal road	$3 \times 10^{-8} - 800 \times 10^{-8}$	50×10^{-8}
Minor road	$50 \times 10^{-8} - 3000 \times 10^{-8}$	500×10^{-8}

6.4 The Kinetic Energy

By definition, the kinetic energy is given by

$$E_k(j\omega) = \frac{1}{2} \int_0^{2\pi} \rho h a b \dot{u}(\theta, j\omega) \dot{u}^*(\theta, j\omega) d\theta, \quad (6.10)$$

where \dot{u} is the velocity of a point of the ring and $(\cdot)^*$ is the complex conjugate operator. The displacement can be related to the modal shape by means of modal

amplitude coefficient a . If the modal coefficient and the ring displacement are collected in the vectors \mathbf{a} and \mathbf{b} , their relationship is

$$\mathbf{u} = \Psi \mathbf{a} \quad \text{and} \quad \mathbf{a} = \Psi^+ \mathbf{u}, \quad (6.11)$$

where $(\cdot)^+$ is the pseudo-inverse operator.

Consequently equation (6.10) becomes

$$E_k(j\omega) = \frac{1}{2} \rho h a b \sum_{n=0}^{\infty} \dot{a}_n \sum_{m=0}^{\infty} \dot{a}_m^* \int_0^{2\pi} \psi_n(\theta, j\omega) \psi_m(\theta, j\omega) d\theta. \quad (6.12)$$

Since the orthogonality properties of the mass-normalised mode shape is given by

$$\rho h a b \int_0^{2\pi} \psi_n(\theta, j\omega) \psi_m(\theta, j\omega) d\theta = \begin{cases} 1 & n = m \\ 0 & n \neq m \end{cases}, \quad (6.13)$$

the following equation for the kinetic energy can then be inferred

$$E_k(j\omega) = \frac{1}{2} \sum_{n=0}^{\infty} \dot{a}_n \dot{a}_n^* = \frac{1}{2} \text{trace}\{\dot{\mathbf{a}} \dot{\mathbf{a}}^H\}, \quad (6.14)$$

Substituting equation (6.11) and applying the expected value operator the following equation may be obtained

$$E_k(j\omega) = \frac{1}{2} \text{trace}\{\Psi^+ \mathbf{S}_v \Psi^{+H}\}. \quad (6.15)$$

Figure 4 shows the kinetic energy evaluated at different car speeds, which illustrates that as well as an overall increase in level, greater speeds also tends to emphasise the resonant response at about 100 Hz.

6.5 The Application of the Optimal Control Filter

Using the properties of the trace operator equation (6.19) can be expressed also as

$$E_k(j\omega) = \frac{1}{2} \text{trace}\{\Psi^{+H}\Psi^+\mathbf{S}_{vv}\}. \quad (6.16)$$

It follows then that defining

$$\mathbf{Q} = \frac{1}{2} \Psi^{+H}\Psi^+, \quad (6.17)$$

and using the results of section 5, the optimal feed-forward control can be designed to minimise the kinetic energy of the ring (Elliott, 2001).

Figure 5 shows the effect of the controller on the kinetic energy for a particular road velocity and one particular position of the force actuator which extends over five grid points, centred at 60° from horizontal on the side of the tyre following the control patch. Two kinds of control strategies have been applied that depends on the way in which the forces are applied at the control points. In first instance a controller as been considered that applies the same force at all the points. In second instance an independent force has been applied at each point to give a multi dof control system. The former controller has been considered in order to investigate the effect of distributed actuator, although the effects are similar to those of a single force actuator acting on the centre grid point. The distributed actuator acting at this location, however only gives an overall reduction of about 4dB. It can be seen that the effect of five independent forces is much greater than a single distributed force, giving an overall reduction of about 25 dB in this frequency range.

However the use of five independent actuators is very difficult to implement. Hence attention has been focused on modelling different kinds of real actuators to be used individually. Three different kinds of actuators have been considered: a distributed force actuator, that might be implemented with an electromagnet for example, a strain actuator, that might be implemented with a piezo-ceramic device for example, and an

acoustic actuator, that might be implemented with a loudspeaker inside the tyre. Figure 6 shows a schematisation of these actuators. The force actuator exerts a radial force at the tread whereas the strain actuator generates a pair of tangential forces at the tread. The acoustic actuator exerts a pressure around the tyre with a sinusoidal distribution corresponding to the first acoustic mode of the tyre interior, so that it couples into the vertical displacements of the tyre. The attenuation in the global kinetic energy that can be obtained for each of these actuators has been computed and Figure 7 shows as such reduction varies with the angular position at which the actuator is placed, being greater when the actuator is near the contact patch, that extends from an angular position of $\pm 5.8^\circ$ in this model.

Figure 7 shows that potentially a large reduction can be obtained in the kinetic energy using either force or acoustic actuators. Such results demonstrate the validity and efficiency of the methodology explained in this report. They are, however, very preliminary and there is a long way to go before such methodology can be validated and applied to the real case. The model of the tyre and that of the actuators used here are very simplified, and permit only an intuitive and qualitative evaluation of the method. Therefore not too much importance should be given to the numerical values, since both the model of the tyre and that of the actuators need to be validated by experimental tests.

7. Conclusions

Tyre contact dynamics are generally nonlinear, because not all of the tyre is in contact with the road at any one time. The relative displacement between the tyre and the road thus creates a contact force if it is negative but creates no contact force if it is positive. In general the contact force has to be calculated using iterative techniques, and because the secondary forces would influence the tyre's motion in the contact patch, a full nonlinear model would have to be solved at each instant in time to accurately determine the effect of active control. If the tyre is assumed to be smooth, however, and sufficiently soft that all of the tyre's surface is in contact with the road surface in the contact patch, the contact model becomes linear and exact results for the effect of active control can be obtained analytically. The contact patch is modelled with an array of radial springs to approximate a Winkler bedding, but the tangential excitation due to friction has not been accounted for.

This linear model can be used to calculate the vibration velocity of the tyre due to both road excitation, specified by the spectral density matrix of a set of road displacements, and to a set of controllable secondary force distributions. A feedforward control formulation can then be used to estimate the minimum response of the tyre on a particular road surface with a particular secondary actuator.

The formulation is illustrated with the preliminary results of a calculation for the kinetic energy of a two-dimensional tyre model running over a rough road at different speeds and being controlled by a secondary force. Such a two-dimensional ring model is only realistic up to about 300 Hz, above which a full three-dimensional model would need to be used. It does however allow the low frequency response of the tyre to a rough road to be calculated for various road speeds, although the current model does not account for rotation of the tyre. Initial results are also presented for the performance of different types of actuators used to minimise the tyre's kinetic energy using an idealised, feed-forward controller. Useful reductions are predicted for a force actuator acting close to the contact patch and for an acoustic actuator, although the required authority of these actuators has not yet been calculated and many practical problems need to be overcome before such active systems could be tested in practice.

A. A brief explanation of some ring models

The tyre model used in the simulation is the stationary ring model proposed by Soedel (1993). The dynamics of such a model is described by equations (6.1) and (6.2). In such a model the stiffness of the sidewalls, the inflation pressure and the loss factors of sidewalls, tread and internal pressure have been taken into account. The stiffness of the sidewalls have been modelled by a massless foundation characterised by two spring constants, k_r and k_θ , that are respectively a radial and a tangential stiffness. Such a model does not take into account the stiffness of the suspension, nor the effects due to the rotation. The effects of the rotation are mainly the stiffening of the tread due to the centrifugal force, the Doppler shift due to the Coriolis term and the horizontal force on the hub due to the free vibration of the tread after leaving the contact patch. However the effect of the centrifugal force can be taken into account adding to the pressure a centrifugal component equal to $\rho h a \Omega^2$ where Ω is the rotating speed.

For a closed ring the solution of such equations will be of the form:

$$u_r(\theta, t) = A_n \cos n(\theta - \phi) e^{j\omega t}, \quad (\text{A.1})$$

$$u_\theta(\theta, t) = B_n \sin n(\theta - \phi) e^{j\omega t}. \quad (\text{A.2})$$

Differentiating such trial solution with respect to time, posing the external load q_r and q_θ to zero and substituting in equations (6.1) and (6.2), the following systems can be obtained:

$$\begin{bmatrix} \alpha_{11} - \rho h \omega_n^2 & \alpha_{12} \\ \alpha_{21} & \alpha_{22} - \rho h \omega_n^2 \end{bmatrix} \begin{Bmatrix} A_n \\ B_n \end{Bmatrix} = \begin{Bmatrix} -P_0 \\ \cos(n\theta) \\ 0 \end{Bmatrix}, \quad (\text{A.3})$$

where

$$\alpha_{11} = \frac{D}{a^4} n^4 + \frac{K}{a^2} + \frac{P_0}{a} (n^2 + 1) + k_r \quad (\text{A.4})$$

$$\alpha_{12} = \frac{D}{a^4} n^3 + \frac{K}{a^2} n + \frac{2P_0}{a} n \quad (\text{A.5})$$

$$\alpha_{12} = \alpha_{21} \quad (\text{A.6})$$

$$\alpha_{22} = \frac{D}{a^4} n^2 + \frac{K}{a^2} n^2 + \frac{P_0}{a} (n^2 + 1) + k_\theta. \quad (\text{A.7})$$

The pressure P_0 has two effects on the ring dynamics. The first one is as an external load and is described by the term in the right hand side of equation (A.3). This term must be neglected in order to find the free mode shapes of the system. The second effect of the pressure is the increase in the stiffness membrane and this must be considered.

In order to obtain the natural frequencies of the ring, the determinant of the coefficients matrix of equation (A.3) has to be posed to zero, that is

$$\omega_n^2 = \frac{(\alpha_{11} + \alpha_{22}) \pm \sqrt{(\alpha_{11} + \alpha_{22})^2 - 4(\alpha_{11}\alpha_{22} - \alpha_{12}\alpha_{21})}}{2\rho h}. \quad (\text{A.8})$$

Given the natural frequencies, the mode shapes can be obtained by one of the following relationship

$$\frac{B_n}{A_n} = \frac{\rho h \omega_n^2 - \alpha_{11}}{\alpha_{12}} \quad \text{or} \quad \frac{A_n}{B_n} = \frac{\rho h \omega_n^2 - \alpha_{22}}{\alpha_{21}}. \quad (\text{A.9})$$

In order to mass-normalise the mode shape the modal mass of each mode can be obtained by the following integration:

$$m_n = \rho b h a \int_0^{2\pi} (u_{rn}^2 + u_{\theta n}^2) d\theta. \quad (\text{A.10})$$

Once the mode shape matrix has been computed the mobility α_{jk} between two points on the ring j and k can be written as

$$\alpha_{jk} = \sum_{n=0}^N \frac{\Psi_{jn} \Psi_{kn}}{\omega_n^2 - \omega^2}. \quad (\text{A.11})$$

For each natural frequencies there are two mode shapes, which are shifted in space of an angle that is $\pi/2n$.

Besides the dynamical model described by equations (6.1) and (6.2), other models have been proposed. For instance Heckl (1986) and Kropp (1989) preferred to use the following model:

$$\frac{D}{a^4}(u_r''' + u_r') - \frac{K}{a^2}(u_r' + u_\theta'') + k_\theta u_\theta + \rho h \ddot{u}_\theta = 0 \quad (\text{A.12})$$

$$\frac{D}{a^4}(u_r'''' + u_r'') + \frac{K}{a^2}(u_r + u_\theta') - \frac{P_0}{a}(u_r + u_r'') + k_r u_r + \rho h \ddot{u}_r = q_r. \quad (\text{A.13})$$

Such models present some simplifications in the main term due in part to the inextensional approximation. Such a model has also been considered here but not many differences in the results have been observed. Such a model has been proven to fit well to experimental results as shown by Kropp (1989). The model is still given by a stationary ring resting on a massless elastic foundation so that it takes into account the sidewalls stiffness and the internal pressure. Again the model does not take into account the effects of rotation and the suspension stiffness.

Kung et al. (1986) described a simplified elastic ring-spring model where the tyre was modelled as a circular, elastic ring supported by distributed spring in both radial and tangential direction. Neither internal pressure nor rotation effects were taken into account. They improved the simple ring model by considering the hub and modelling it as a rigid mass to which the distributed spring was attached.

Huang and Soedel (1987) also examined the effect of rotation on the system characteristic. Applying Hamilton's principle to a rotating ring on an elastic foundation, the following equation can be obtained:

$$\frac{D}{a^4}(u_r''' - u_\theta''') - \frac{K}{a^2}(u_r' + u_\theta'') + \frac{P_0}{a}(u_\theta - 2u_r' - u_\theta'') + k_\theta u_\theta + \rho h(\ddot{u}_\theta + 2\Omega\dot{u}_r - \Omega^2 u_\theta) = q_\theta \quad (\text{A.14})$$

$$\frac{D}{a^4}(u_r''' - u_\theta''') + \frac{K}{a^2}(u_r + u_\theta') + \frac{P_0}{a}(u_r + 2u_\theta' - u_r'') + k_r u_r + \rho h(\ddot{u}_r - 2\Omega\dot{u}_\theta - \Omega^2 u_r - a\Omega^2) = q_r - P_0, \quad (\text{A.15})$$

where Ω is the rotating speed of the ring. Since the rotating speed takes into account only the Coriolis effect, the centrifugal effect must be taken into account by adding a uniform pressure $P_0 = \rho h a \Omega^2$. In general, for each value of n greater than zero, there are four distinct natural frequencies, ω_{nk} , $k = 1, 2, 3, 4$, wherein two are the bifurcations resulting from the Coriolis acceleration. This is different from the non-rotating case in which only two frequencies exist. Two of the four natural frequencies obtained are associated with predominantly inextensional (transverse) vibration, and the other two are related to the predominantly extensional (circumferential) vibration. The inverted case, where the ring is stationary and a point load travels around it, was also studied for comparison. The travelling load approach does not account for the centrifugal tension and the Coriolis acceleration and as the rotational speed increases it tends to excite the lowest bending mode. When the centrifugal tension and the Coriolis component are considered, the system's natural frequencies increase with rotational speed and the solution yields no resonant speeds.

References

- Dodds, C.J. and Robson, J.D. (1973) The description of road surface roughness. *Journal of Sound and Vibration*, **31**, 175-183.
- Elliott S.J. (2001) *Signal Processing for Active Control*. Academic Press.
- Elliott, S.J., Maury, C. and Gardonio, P. (2004) The synthesis of spatially correlated random pressure fields. To be published in *Journal of the Acoustical Society of America*.
- Heckl, M. (1986) Tyre noise generation. *Wear*, **113**, 157–170.
- Huang, S.C. and Soedel, W. (1987) Effects of coriolis acceleration on the free and forced in-plane vibrations of rotating rings on elastic foundation. *Journal of Sound and Vibration*, **115**(2), 253–274.
- Johnson, K.L. (1985) *Contact Mechanics*, Cambridge University Press.
- Koopman, G.H. and Farelane J.B. (1997) *Designing Quiet Structures*. Academic Press.
- Kropp W., Larsson K., Wallens F. and Andersson P. (2004) Tyre/road noise generation – modelling and understanding. *Proc. Institute of Acoustics*, **26**, pt.2, 1-12.
- Kropp, W. (1989) Structure-borne sound on a smooth tyre. *Applied Acoustics*, **26**, 181-192.
- Kung, L.E. Soedel, W and Yang, T.Y. (1986) Free vibration of a pneumatic tire-wheel unit using a ring on an elastic foundation and a finite element model. *Journal of Sound and Vibration*, **107**(2), 181–194.
- Larsson, K. (2002) *Modelling of dynamic contact – exemplified by the tyre/road interaction*. PhD thesis. Chalmers University.
- Newland, D.E. (1984) *An Introduction to Random Vibrations and Spectral Analysis*. Longman Scientific & Technical, 2nd edition,.
- Robson, J.D. (1979) Road surface description and vehicle response. *International Journal of Vehicle Design*, **1**, 23-35.
- Soedel, W. (1993) *Vibrations of Shells and Plates*. Marcel Dekker, Inc., New York, 2nd edition.

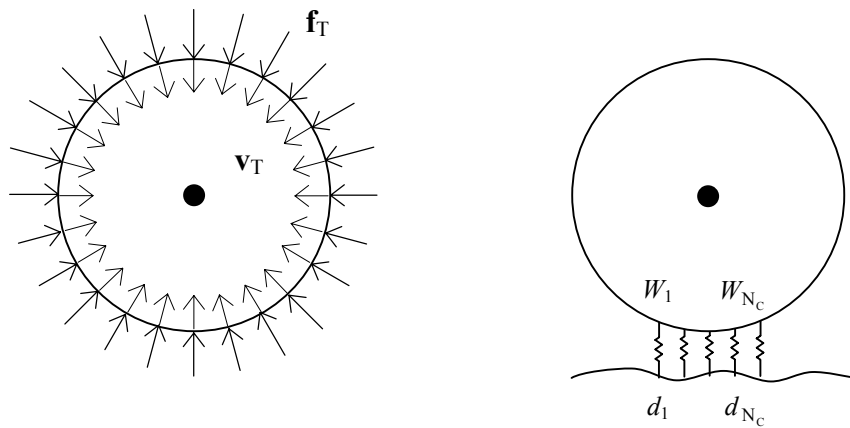


Figure 1. The radial velocities of the tyre, \mathbf{v}_T , suspended off the road, are related to the applied forces, \mathbf{f}_T , via the mobility matrix \mathbf{Y}_F (left hand figure). When the tyre is resting on the road (right hand figure), a Winkler bedding model of the contact patch is used, excited by the displacements of the road, \mathbf{d} , and generating vertical displacements of the tyre in the contact patch, \mathbf{w} .

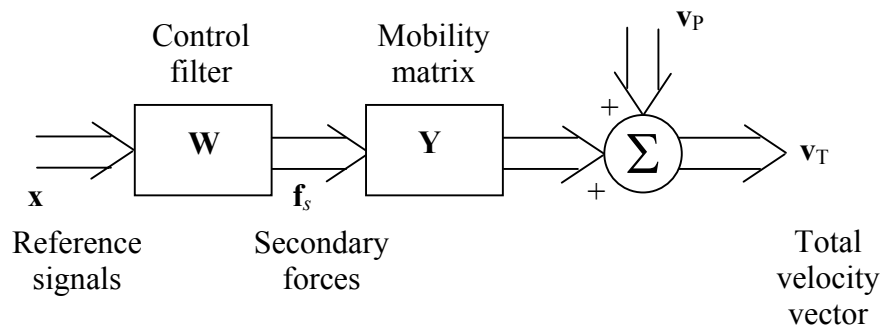


Figure 2. Block diagram for the active control formulation.

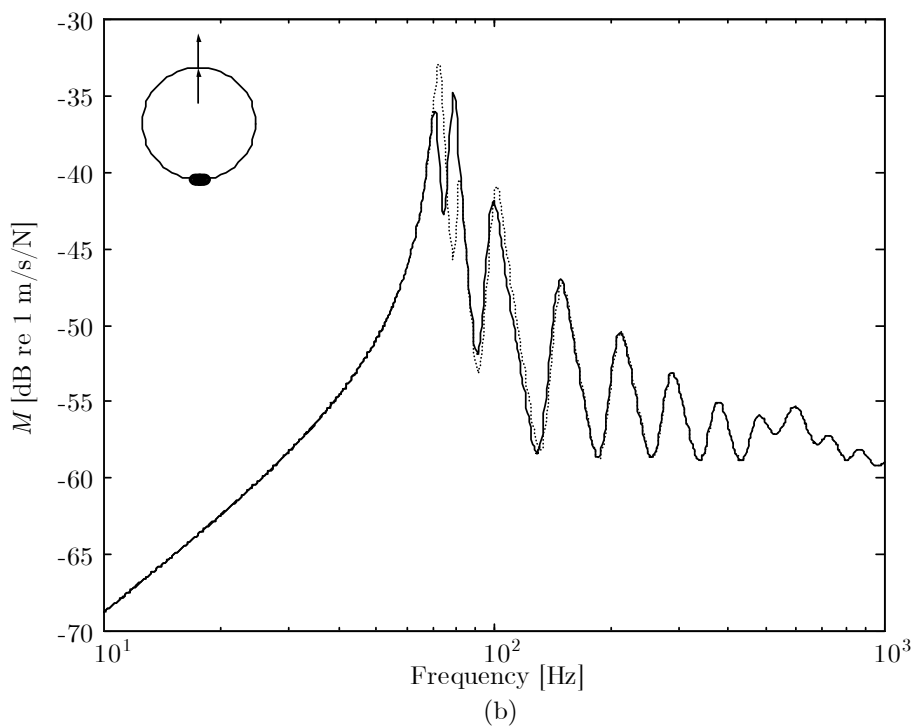
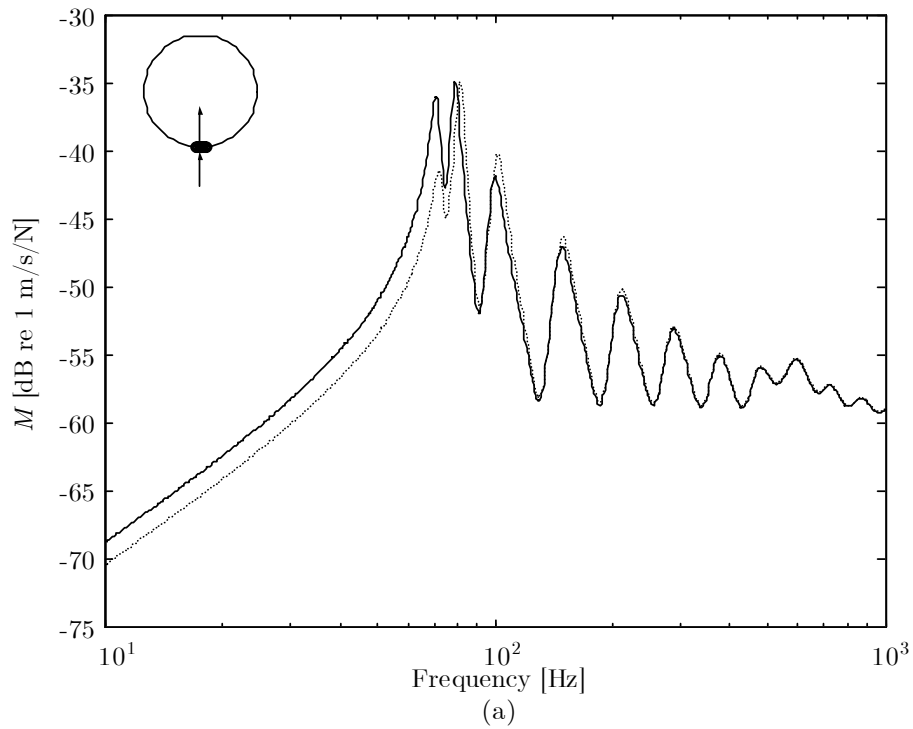


Figure 3. Effect of the road contact on the tyre point mobility calculated in the middle of the contact patch (a) and opposite to the contact patch (b): — hanged tyre; - - - tyre on ground.

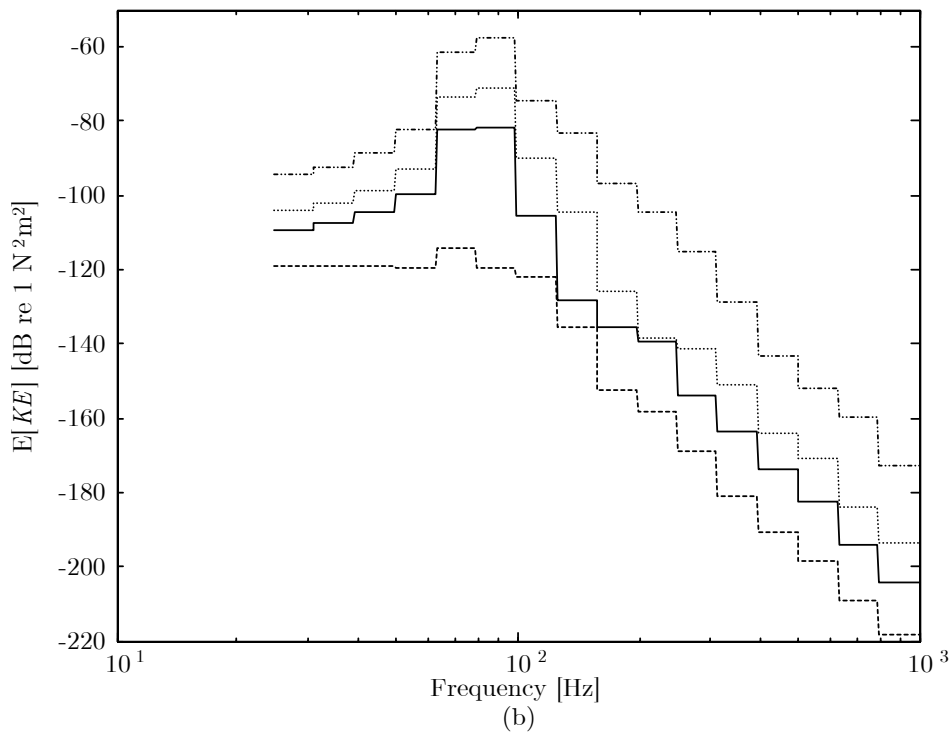
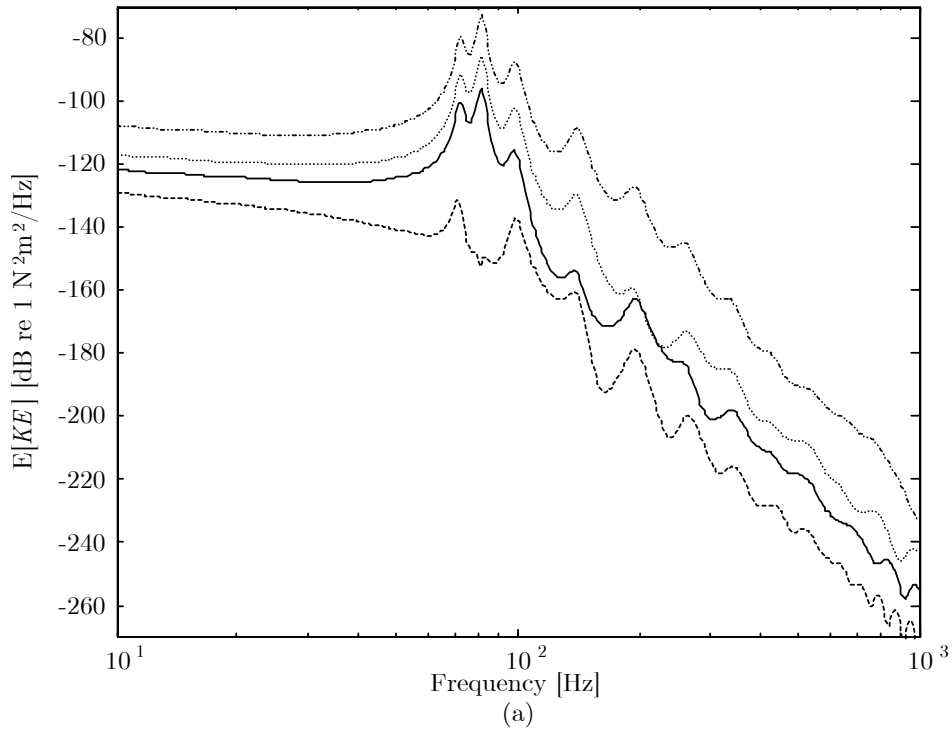


Figure 4. Expected value of the kinetic energy, shown in the form of power spectrum density (a) and one-third octave bands (b), evaluated at different car speeds: - - - 100 km/h; ··· 50 km/h; — 35 km/h; - - - 20 km/h.

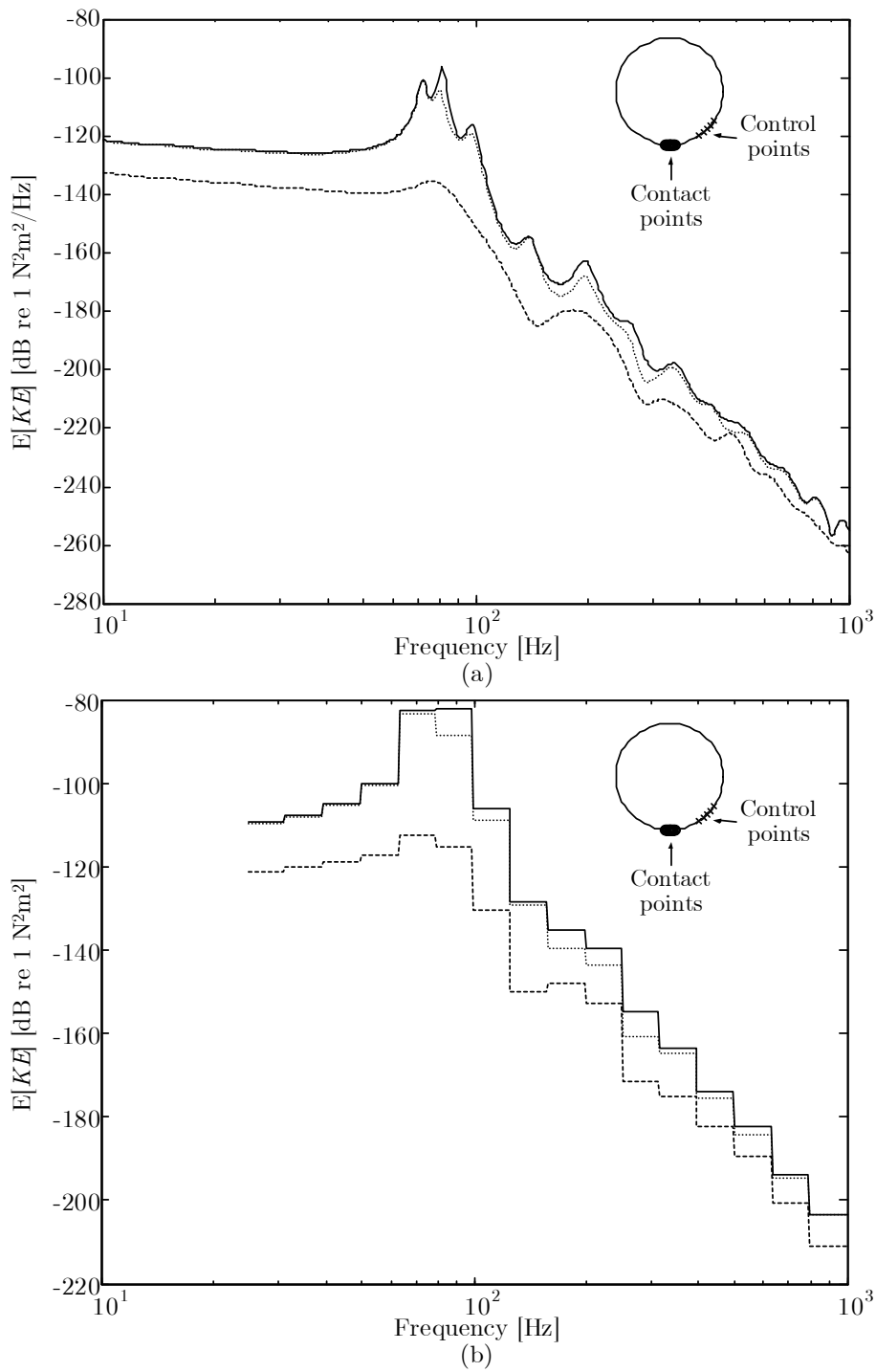


Figure 5. Expected value of the kinetic energy, shown in the form of power spectrum density (a) and one-third octave bands (b) for a speed of 35 km/h: — controller off, $\cdot \cdot \cdot$ uniform control on and - - - multi dof control on.

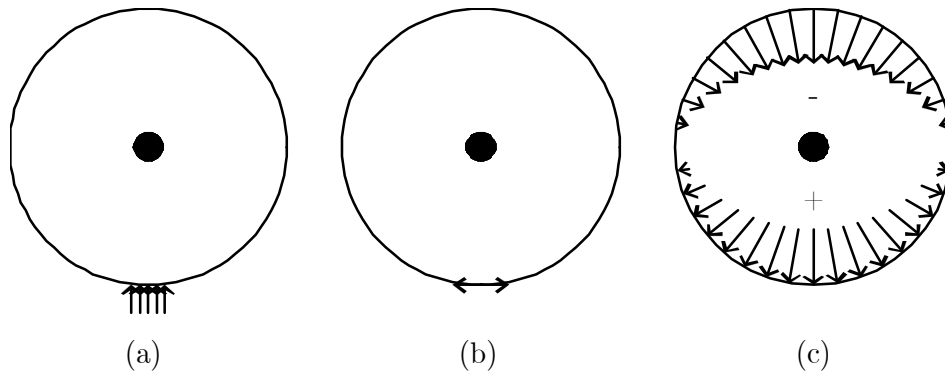


Figure 6. Modelling of the different kinds of actuators: distributed force actuator (a), strain actuator (b) and acoustic actuator (c).

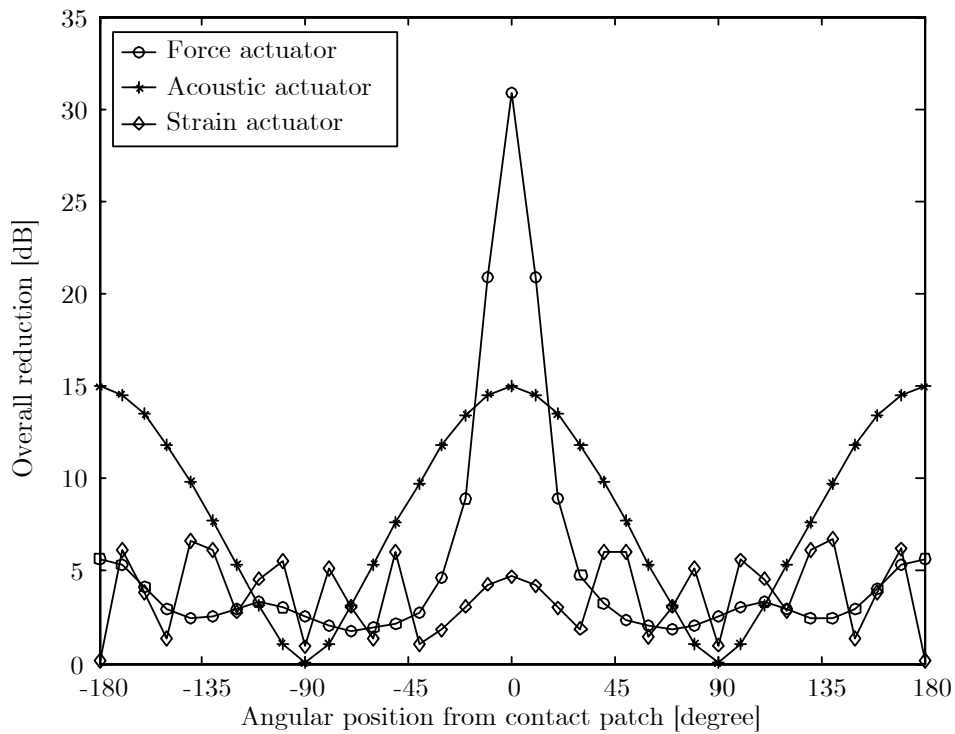


Figure 7. Influence of the position of the actuator on reduction of the global kinetic energy.